# J2.4 METEOROLOGICAL UNCERTAINTY EFFECTS IN ATMOSPHERIC TRANSPORT AND DISPERSION MODELING: A DEMONSTRATION

L. Joel Peltier*, Sue Ellen Haupt, John C. Wyngaard
David Stauffer, Aijun Deng, Francis Kredensor

The Pennsylvania State University, State College, PA

## 1. INTRODUCTION

The atmospheric dispersion of a contaminant is a complicated physical process involving a three-dimensional, turbulent wind field with a very wide range of spatial scales. This wind field is affected by the physical features and the energy balance of the underlying surface, and by the large-scale atmospheric conditions. The instantaneous, local state of this turbulent wind field is chaotic and cannot be predicted with certainty (Wyngaard 1992, Wyngaard and Peltier 1996). But the atmospheric dispersion of contaminants by the wind field is an important contemporary problem that must be addressed. Examples include emission plumes from industrial complexes, smoke stacks, and traffic sources; chemical plumes from accidental releases; and chemical, biological, nuclear, or radiological clouds from deliberate releases (National Research Council 2003).

Some atmospheric transport and dispersion models couple a representation of the contaminant source with an estimate of the expected (i.e., ensemble-mean) wind field to predict the expected contaminant trajectory and strength and an estimate of the expected hazard area. These statistical predictions have uncertainty bounds which are seldom quantitatively known.

The average dispersion caused by turbulence that differs from realization to realization within an ensemble could be called "virtual dispersion," to use G. I. Taylor's term, in that it exists only as an average over many realizations. To illustrate, imagine a nondeformable, nondiffusive puff of effluent (a neutrally buoyant balloon, for example) released into a turbulent flow. Within each realization this balloon follows a different turbulent trajectory in response to the local wind field. Averaging over a large ensemble of realizations yields a mean concentration field that in its broad, diffuse nature and much-lower concentrations clearly displays this virtual dispersion.

Wind fields can be diagnosed from a variety of sources and their fidelity can range widely. Those derived from observations have highest fidelity nearest the observation stations and measurement times and increasing uncertainty as the spatial and temporal separations increase. The uncertainty depends on the quality of the interpolation between stations. Wind-field models coupled with observations can minimize the interpolation error in space and time. Diagnostic models enforce realizability constraints on the interpolated wind fields to improve their fidelity. The prognostic models used in numerical weather prediction (NWP) produce wind fields that are consistent with the modeled governing equations, the imposed boundary conditions and forcings, and the observational data assimilated into the model system.

Data assimilation is a critical step toward minimizing wind-field uncertainty. The space comprising all possible wind fields consistent with the governing equations and with the initial and boundary conditions is large. Data assimilation shrinks this space by excluding those members not consistent with available measurement data. The set-average wind field shares the similarities of the surviving members. For historical reconstructions, data-

Corresponding author address: L. Joel Peltier, Applied Research Laboratory, P.O. Box 30, Pennsylvania State University, State College, PA 16804; e-mail: peltierlj@psu.edu

assimilated wind fields can be true to the coherent scales of the actual wind field realization. As time and distance from the point of data insertion increases the predicted wind field departs from the actual field and uncertainty increases. The decorrelation time relates to the lifetime of coherent structures in the flow field. Thus wind-field estimates for "nowcasts," 0 to 6 hours into the future, also may be reasonably good, especially when data assimilation is used during a pre-forecast period to improve model spinup (Leidner, et al. 2001, Otte, et al. 2001). With no data available for assimilation, wind estimates for forecasts 24 or more hours into the future revert to the ensemble of all consistent wind-field members.

The wind field introduces two scale-based types of uncertainty into a dispersion prediction. One is the uncertainty in the wind field used to transport the contaminant. We call this "outer variability". The second is the unresolved turbulence within this transporting wind field ("inner variability"). Although some models such as SCIPUFF (Second order Closure Integrated Puff model) (Sykes, et al. 1984, Sykes 2004) include a parameterization of the inner variability in terms of large-scale variability (LSV) parameters, they do not specifically include the outer variability. We propose approaches to parameterizing this outer variability that are based on ensembles of meteorological forecasts. The concept is that the uncertainty in the transporting wind field can be diagnosed from an ensemble of wind-field predictions, allowing one to compute uncertainty fields from the ensemble and extract uncertainty parameterization information from them.

This paper is organized as follows. First we consider data-assimilated model output in the context of ensemble-averaging concepts. We then derive a dynamical equation for the evolution of the outer variability velocity scale and propose a model equation for its spatial scale. This provides an uncertainty representation that can be used in atmospheric dispersion models.

## 2. ASSESSING WIND-FIELD UNCERTAINTY

Because turbulent flows have what is called ``sensitive dependence on initial conditions," their evolving details in a particular realization cannot be predicted with certainty (Lorenz 1963). Experience shows, however, that in sufficiently well understood flows the flow statistics can often be predicted reasonably well. Thus dispersion models are designed to predict ensemble average dispersion statistics (National Research Council 2003).

Fig. 1 illustrates these points by depicting the differences between the instantaneous structure in a realization of a turbulent flow (panel a) and the ensemble-mean flow (panel b), using a dispersing plume for flow visualization. Panel a is a snapshot in time; a snapshot taken a short time later would be shifted downstream but otherwise be similar because the large-scale structure changes slowly. A snapshot taken much later would be very different. The snapshot is one member of the ensemble of possible realizations for the concentration field, each denoted by $\tilde{c}(\vec{x},t;n)$, where *n* is realization number, $\vec{x}$ is spatial position, and $t$ is time. Common characteristics of each member of the ensemble are highly concentrated effluent regions separated from "clear" surrounding fluid, and spatial variability that increases with distance from the source. Were one to stand in a plume's path, one would experience moments of very high exposure separated by times of minimal exposure.

The ensemble-mean flow, Fig. 1b, is the average over all realizations. Its concentration field $C(\vec{x},t)$, is

$$C(\vec{x},t) = \lim_{N\to\infty} \frac{1}{N} \sum_{n=1}^{N} \tilde{c}(\vec{x},t;n) \qquad (1)$$

and differs significantly from the concentration fields of the individual members. The local pockets of high concentration and downstream variability disappear in the averaging; the mean plume is symmetric about the centerline and has uniformly decreasing concentration with increasing downstream distance. The mean field is stationary; it has no large-scale intermittency.

The statistics of the fluctuating field, $c(\vec{x},t;n) = \tilde{c}(\vec{x},t;n) - C(\vec{x},t)$, provide measures of the concentration variability. The concentration variance is a commonly used metric:

$$\overline{c^2}(\vec{x},t) = \lim_{N\to\infty} \frac{1}{N} \sum_{n=1}^{N} c(\vec{x},t;n) . \quad (2)$$

The greater the variability between the ensemble members, the greater the variance.

Models can be developed and calibrated to predict the statistics of the ensemble-mean plume, but that plume will not be observed in any realization: it is a "virtual plume." If, however, in a dispersion problem the ensemble-mean outcome is acceptable, the ensemble-mean wind field is appropriately used to drive the model. Dispersion problems involving long-duration releases, which are often called chronic problems, are an example. Short-duration releases, called acute or episodic problems, are sensitive to details of the transporting wind field, and ideally the transporting wind field would be the one experienced during the event. In practice it should be our best estimate of that field.

Figure 1c represents a transporting wind field appropriate for modeling the acute release in Fig. 1a. The red circles in the figure represent measurement stations that give some knowledge of the wind field during the release. Data-assimilated NWP predictions for this flow, using observations from these stations as input, isolate a subspace of the wind field ensemble that comprises those realizations that are consistent with the data. Because observation stations are sparse, and initial and boundary conditions are not known exactly, and the physical models underlying the NWP system are approximate, data-assimilated NWP will not uniquely identify the member in Fig. 1a as the transporting wind field. Instead, it will identify a number of members that have common large-scale features but differ in detail. Denoting the conditionally sampled subspace by $\tilde{c}(\vec{x},t;\eta)$, where $\eta$ is the subspace member number, the conditionally averaged plume concentration is

$$\tilde{C}(\vec{x},t) = \lim_{N\to\infty} \frac{1}{N} \sum_{\eta=1}^{N} \tilde{c}(\vec{x},t;\eta) . \quad (3)$$

$\tilde{C}(\vec{x},t)$ will correlate well with the actual plume in Fig. 1a because they will have common features. $\tilde{C}(\vec{x},t)$ will exhibit large-scale variability, but its small-scale structure will be more diffused and the boundary between the plume and the surrounding fluid will be less sharp.

Even though the structure of the conditionally averaged plume is similar to the structure of a realization, as a statistical construct the conditionally averaged plume cannot be realized, although its differences from a realizable plume are much less distinct. The inter-member variability of subspace $\tilde{c}(\vec{x},t;\eta)$ is a measure of prediction uncertainty. It can be much less than the full ensemble variability, depending on the NWP skill, and will asymptote (in time) to the full ensemble variability for forecasts as time from the last available data-assimilation instant increases.

Although the discussion above focuses on the concentration field as an example, our statements apply equally well to the velocity field and to other transported quantities. The primary points are 1) wind-field ensembles provide one route for assessing the effects of wind-field uncertainty on dispersion, 2) representations of the mean wind field may be adequate for modeling chronic releases but not for modeling acute releases, and 3) dispersion-model uncertainty can be mitigated by numerical weather prediction skill.

## 3. LARGE-SCALE UNCERTAINTY MODELING

Large-scale uncertainty effects on dispersion are generally not predicted by contemporary dispersion models. A traditional approach is to use one representation of the transporting wind field coupled with one representation of the source to make one prediction of the dispersion event. Depending on the sophistication of the dispersion model, some effects of unresolved motions may be represented. To our knowledge, however, no

dispersion model accounts for the effects of variability of the wind-field ensemble. Most uncertainty analyses are more in the context of sensitivity to input parameters (Rao 2005; Hanna, et al. 1998; Lewellen and Sykes 1989).

Figure 2 presents a research plan for accounting for large-scale uncertainty in dispersion models. The desired capability is to use one wind field to make one dispersion prediction and have large-scale uncertainty effects included through parameterizations. This approach retains quick turn-around for rapid response, while giving better estimates of true hazards. Without appropriate parameterizations, the effects of large-scale uncertainty can be assessed by creating a large-scale wind-field ensemble (a process already used in operational NWP), running dispersion predictions for each ensemble member, then ensemble-averaging the dispersion results. This process is computationally intensive, requiring multiple wind-field representations and multiple dispersion runs, so is not an attractive operational alternative. An intermediate approach is to create the large scale wind-field ensemble, preprocess the ensemble to extract a representative wind field and parameterized uncertainty scales, and then perform one dispersion prediction using the representative wind field and the uncertainty parameters. Because the preprocessing can be completed offline and the uncertainty data stored along with the representative wind field, the latter approach can be made operationally feasible. This intermediate capability is the focus of our work.

The inherent unpredictability of atmospheric flows means that any one representative wind field will have an associated uncertainty. In Fig. 3 (upper panel) we present dispersion results for three members of a wind field with as large as 90° wind-direction uncertainty between them. The individual plumes share common widths and concentration distributions but differ in their orientations. A representative wind direction could be the average, 45°, and the uncertainty scales would relate to the differences in the plume trajectories. The single dispersion prediction using the representative wind direction coupled with the uncertainty scales is presented in Fig. 3 (lower panel). The hazard area of the predicted plume is now much larger, enveloping the region affected by the wind-direction uncertainty.

We have suggested that large scale-uncertainty can be assessed using model nsemble data and have proposed that uncertainty parameters be extracted to represent the effects of large-scale uncertainty in dispersion. Using ensembles is emerging as a new direction in dispersion modeling (Warner, et al. 2002; Galmarini, et al. 2004a,b). The following sections demonstrate this approach, using a contemporary NWP ensemble as a starting point.

### 3.1 Short-Range-Ensemble Forecast (SREF) Data

Our case study is based on a short-range-ensemble forecast for the United States supplied by the National Center for Environmental Prediction (NCEP) (McQueen, et al. 2005.) The SREF results are from 15 model runs initialized two times per day for 48-hour forecasts. Forecasts begun at 1200Z September 21 are chosen as a representative mid-latitude case due to fronts over the eastern United States.

Visualizations of the wind field vectors at the 850mb surface and surface temperature contours are presented in Fig. 4 for the 15 SREF members. A visual scan shows strong similarities among the members (as desired because each is a ``best prediction" of the expected weather). Differences exist as well; they relate to the effects of model error, initial and boundary condition sensitivity, and solution drift due to nonlinearities in the governing equations.

The variability within the ensemble is directly related to the large-scale uncertainty. Defining the member velocity, $U_i^n$, and the mean velocity, $U_i$, where

$$U_i(\vec{x},t) = \lim_{N\to\infty} \frac{1}{N} \sum_{n=1}^{N} U_i^n(\vec{x},t;n) \quad (4)$$

a deviation velocity, $\delta U_i^n = U_i^n - U_i$, can be defined that is nonzero only when variability in

the ensemble exists. Scalar measures of the uncertainty are the deviation energy,

$$\delta k = \lim_{N\to\infty} \frac{1}{N}\sum_{n=1}^{N} \frac{1}{2}\delta U_i^n U_i^n = \frac{1}{2}\overline{\delta U_i^n U_i^n}\ , \quad (5)$$

and the corresponding characteristic velocity, $q_L = \sqrt{\delta k}$ . The subscript "L" is used to denote "large-scale variability."

The mean velocity vectors and mean surface temperatures from the SREF ensemble are presented in the left panel of Fig. 5. The characteristic velocity $q_L$ is presented on the right. One sees that the prediction uncertainty, $q_L$, is large in the northeast and southwest quadrants of the plot. A comparison with the surface temperature field suggests that the regions of high uncertainty are associated with frontal systems, as one might expect.

Although $q_L$ provides quantitative information on large-scale uncertainty, it provides no information about its effects on the expected hazard area. For this purpose a second modeling parameter, an uncertainty length scale $\Lambda_L$, is useful. We will show that our parameterization of large-scale uncertainty in terms of characteristic velocity and length scales, $q_L$ and $\Lambda_L$, is equivalent to stating that the effects of large-scale uncertainty on dispersion is diffusive with a characteristic diffusivity given by $\nu_L \sim q_L \Lambda_L$.

### 3.2 A Model for $\Lambda_L$

The member velocity fields in the SREF ensemble each satisfy the momentum equation

$$\frac{\partial U_i^n}{\partial t} + U_j^n \frac{\partial U_i^n}{\partial x_j} = -\frac{1}{\rho}\frac{\partial P^n}{\partial x_i} - \frac{\partial \tau_{ij}^n}{\partial x_j} + \beta_i\ . \quad (6)$$

Here $\beta_i$ represents buoyancy and Coriolis forces, $P^n$ is pressure, and $\tau_{ij}^n$ is a stress tensor that represents the effects of unresolved motions; it is modeled in the NWP code. Averaging (1) over the SREF ensemble (15 runs) yields the mean-velocity transport equation

$$\frac{\partial U_i}{\partial t} + U_j \frac{\partial U_i}{\partial x_j} = -\frac{1}{\rho}\frac{\partial P}{\partial x_i} - \frac{\partial \overline{\tau_{ij}^n}}{\partial x_j} - \frac{\partial \overline{\delta U_i^n \delta U_j^n}}{\partial x_j} + B_i \quad (7)$$

Here P is averaged pressure, $B_i$ is averaged buoyancy and Coriolis forces, and $\partial\overline{\delta U_i^n \delta U_j^n}$ is the kinematic "deviation-field stress" caused by the velocity-deviation fields. We can diagnose this term from the SREF ensemble data. We can also model its diffusive effects, thus providing a means to diagnose the model parameters from the SREF data. We work with the deviation energy $\delta k$ because it is a scalar that yields the model velocity scale.

By subtracting (7) from (6) we form the transport equation for the deviation velocity in the n-th member of the SREF ensemble:

$$\frac{\partial \delta U_i^n}{\partial t} + U_j^n \frac{\partial \delta U_i^n}{\partial x_j} = -\frac{1}{\rho}\frac{\partial \delta P^n}{\partial x_i} - \frac{\partial \delta \tau_{ij}^n}{\partial x_j} + \delta\beta_i^n - \delta U_j^n \frac{\partial U_i}{\partial x_j} - \frac{\partial}{\partial x_j}\left(\delta U_i^n \delta U_j^n - \overline{\delta U_i^n \delta U_j^n}\right) \quad . \quad (8)$$

By contracting (8) with $\delta U_i^n$, averaging over the SREF ensemble, and simplifying we can write

$$\frac{\partial \delta k}{\partial t} + U_j^n \frac{\partial \delta k}{\partial x_j} = -\frac{1}{\rho}\frac{\partial}{\partial x_i}\overline{\delta U_i^n \delta P^n} + \overline{\delta U_i^n \delta\beta_i^n} + \frac{\partial}{\partial x_j}\overline{\delta U_i^n \delta\tau_{ij}^n} - \overline{\delta\tau_{ij}^n \frac{\partial \delta U_i^n}{\partial x_j}} - \overline{\delta U_i^n \delta U_j^n} S_{ij} - \frac{1}{2}\frac{\partial}{\partial x_j}\overline{\delta U_j^n \delta U_i^n \delta U_i^n} \quad (9)$$

where $S_{ij} \equiv \frac{1}{2}\left(\frac{\partial U_i}{\partial x_j} + \frac{\partial U_j}{\partial x_i}\right)$ is the strain-rate tensor associated with the SREF ensemble.

Equation (9), which is formally exact, governs the production, destruction, and transport of deviation energy. By interpreting this equation we can understand the nature of the variability in the SREF ensemble thus understand its uncertainty.

The left side of (9) is the derivative following the mean (over the SREF ensemble) motion. It shows that data advecting through a region of high uncertainty will become less certain and will carry the increased uncertainty to other regions in the flow field. On the right side of (9) are sources of uncertainty. Terms 1, 3, and 6 are flux-divergence terms. They integrate to zero globally, so they can only mix. As contractions of a kinematic stress and a strain-rate tensor, Terms 4 and 5 have the form of production or destruction terms. Term 2 relates to production or destruction of uncertainty through buoyancy and Coriolis forces, but in principle the buoyancy effects can be negligible and one can show that the Coriolis effects vanish identically. It follows that terms 4 and 5 are the key ones in Eq. (9). Term 5 represents the production of uncertainty through the stress of the deviation motion acting on the mean strain rate. Also, the physical modeling for the SREF members is intended to be accurate, so even though inter-model variability exists, we believe that gradient production is the dominant source.

Following the practice in turbulence modeling, we relate the deviatoric stress associated with the deviation motion to the mean strain rate $S_{ij}$ through an effective diffusivity:

$$T_{ij}^D \equiv \left( \overline{\delta U_i^n \delta U_j^n} - \frac{2}{3} k \, \delta_{ij} \right) = -2 \nu_L S_{ij} \,. \quad (10)$$

This modeling assumption leads to an expression for the uncertainty scale $\Lambda_L$. Because the tensor relationship (10) does not yield a unique scalar value for $\nu_L$ (there are 6 independent equations), we perform the additional step of contracting (10) with the deviatoric stress to yield a scalar expression that can give a unique value for $\nu_L$. The relevant steps are:

$$T_{ij}^D T_{ij}^D = -2 \nu_L S_{ij} T_{ij}^D = 4 \nu_L^2 S_{ij} S_{ij} \,, \quad (11)$$

so

$$\nu_L = \sqrt{\frac{1}{4} \frac{T_{ij}^D T_{ij}^D}{S_{ij} S_{ij}}} \,. \quad (12)$$

The right side of (12) can be computed from the SREF ensemble data yielding $\nu_L$. Given $\nu_L$, a characteristic diffusion length, $\ell_L$, can be computed:

$$\nu_L = \ell_L \, q_L = \sqrt{\frac{T_{ij}^D T_{ij}^D}{4 \, S_{ij} S_{ij}}}$$

or

$$\ell_L = \frac{1}{q_L} \sqrt{\frac{T_{ij}^D T_{ij}^D}{4 \, S_{ij} S_{ij}}} \,. \quad (13)$$

The uncertainty model scale $\Lambda_L$ is proportional to $\ell_L$:

$$\Lambda_L = c_L \, \ell_L \,. \quad (14)$$

The proportionality coefficient $c_L$ can be determined by comparisons to diffusion model ensembles.

Figures 6 and 7 present contours of the large-scale diffusivity, $\nu_L$, and large-scale mixing length, $\ell_L$, respectively as diagnosed at the 850mb level of the SREF data. We see that the uncertainty mixing length is on the order of 100 km in the regions of high uncertainty. Similar results were obtained with an analysis at 1000mb. Because we expect the proportionality coefficient to be of order 1, the uncertainty model length scale is also expected to be on the order of 100 km.

## 4. SUMMARY AND DISCUSSION

In this work we present the theoretical basis for using wind-field ensemble data to estimate wind-field uncertainty and present a method for deriving model parameters for uncertainty that can be used in dispersion modeling. The parameters are a characteristic length and

velocity scale that are related to an effective diffusivity for large-scale uncertainty.

The characteristic velocity scale is related to the deviation energy in the wind-field ensemble. By deriving a formally exact transport equation for this energy field, the source term for uncertainty is identified and used to construct a model for the characteristic uncertainty length scale. The SREF data yield an estimate of this parameter on the order of 100 km.

Our future work will consider ensembles of dispersion runs that can be used to tune the proportionality coefficient for our model uncertainty length scale. We intend to use our model in a dispersion code to demonstrate its effectiveness as a representation of large-scale uncertainty in dispersion.

*Acknowledgments*

The authors would like to thank Jeff McQueen of the National Center for Environmental Prediction (NCEP) for providing the SREF data and Ian Sykes of Titan Corporation for helpful discussions. The authors would also like to gratefully acknowledge funding from Defense Threat-Reduction Agency (DTRA) under contract number DTRA01-03-0010, CDR Stephanie Hamilton, Contract Monitor, that made this work possible.

**REFERENCES**

Galmarini, S., et al. (35 additional authors), 2004: Ensemble dispersion forecasting – Part I: application and evaluation, *Atmos. Env*., **38**, 4619-4632.

Galmarini, S., et al. (22 additional authors), 2004: Ensemble dispersion forecasting – Part II: concept, approach and indicators, *Atmos. Env*., **38**, 4607-4617.

Hanna, S.R., J.C. Chang, and M.E. Fernau, 1998: Monte Carlo estimates of uncertainties in predictions by a photochemical grid model (UAM-IV) due to uncertainties in input variables, *Atmos. Env*., **32**, 3619-3628.

Leidner, S.M., D.R. Stauffer and N.L. Seaman, 2001: Improving California coastal zone numerical weather prediction by dynamic initialization of the marine layer. *Mon. Wea. Rev.*, **129**, 275-294.

Lorenz, E.N. 1963: Deterministic Nonperiodic Flow, *J. Atmos. Sciences*, **20**, 130-141.

Lewellen, W.S. and R.I. Sykes, 1989: Meteorological data needs for modeling air quality uncertainties, *J. Atmos. And Oceanic Technology*, **6**, 759-768.

McQueen, J.T., J. Du, B. Zhou, G. Manikin, B. Ferrier, H.-Y. Chuang, G. DiMego, and Z. Toth, 2005: Recent Upgrades to the NCEP Short Range Ensemble Forecasting System (SREF) and Future Plans. 21st Conference on Weather Analysis and Forecasting/17th Conference on Numerical Weather Prediction.

National Research Council, 2003: *Tracking and Predicting the Atmospheric Dispersion of Hazardous Material Releases. Implications for Homeland Security*, The National Academies Press, Washington, D.C.

Otte, T.L. N.L. Seaman and D.R. Stauffer, 2001: A heuristic study on the importance of anisotropic error distributions in data assimilation. *Mon. Wea. Rev.*, **129**, 766-783.

Rao, K.S., 2005: Uncertainty analysis in atmospheric dispersion modeling. *Pure and Applied Geophysics*, **162**, 1893-1917.

Schere, K.L. and C.J. Coats, 1992: A stochastic methodology for regional wind-field modeling, *J. Applied Meteorol*., **31**, 1407-1425.

Sykes, R.I. , W.S. Lewellen, and S.F. Parker, 1984: A turbulent transport model for concentration fluctuations and fluxes, *J. Fluid Mech*., **139**, 193-218.

Sykes, R.I., et al., 2004: SCIPUFF Version 2.0, Technical Documentation, A.R.A.P. Report no. 727, Titan Corp., Princeton, NJ.

Warner, T.T., R.-S. Sheu, J.F. Bowers, R.I. Sykes,, G.C. Dodd, and D.S. Henn, 2002: Ensemble Simulations with Coupled Atmospheric Dynamic and Dispersion Models: Illustrating Uncertainties in Dosage Simulations, *J. Applied Met*., **41**, pp. 488-504.

Wyngaard, J.C., 1992: Atmospheric turbulence. *Annual Review of Fluid Mechanics*, **24**, 205-233.

Wyngaard, J.C. and L.J. Peltier: 1996, Experimental micrometeorology in an era of turbulence simulation, *Bound. Layer Meteor.*, **78**, 71-86.

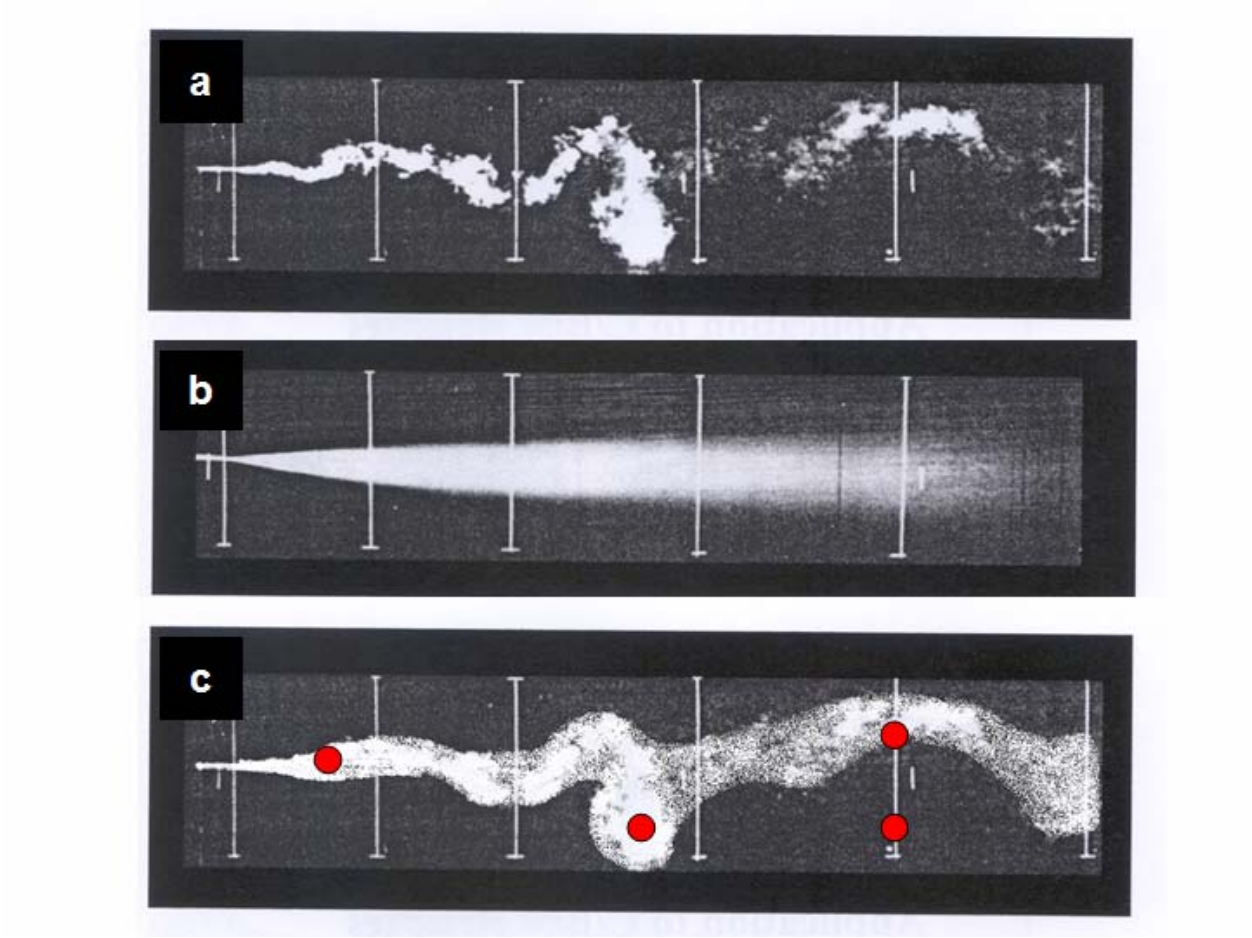


**Figure 1:** Comparison of a) instantaneous, b) long-time average (a surrogate for ensemble-mean) and c) data-assimilated representations of a dispersion plume. The red dots denote measurement stations.

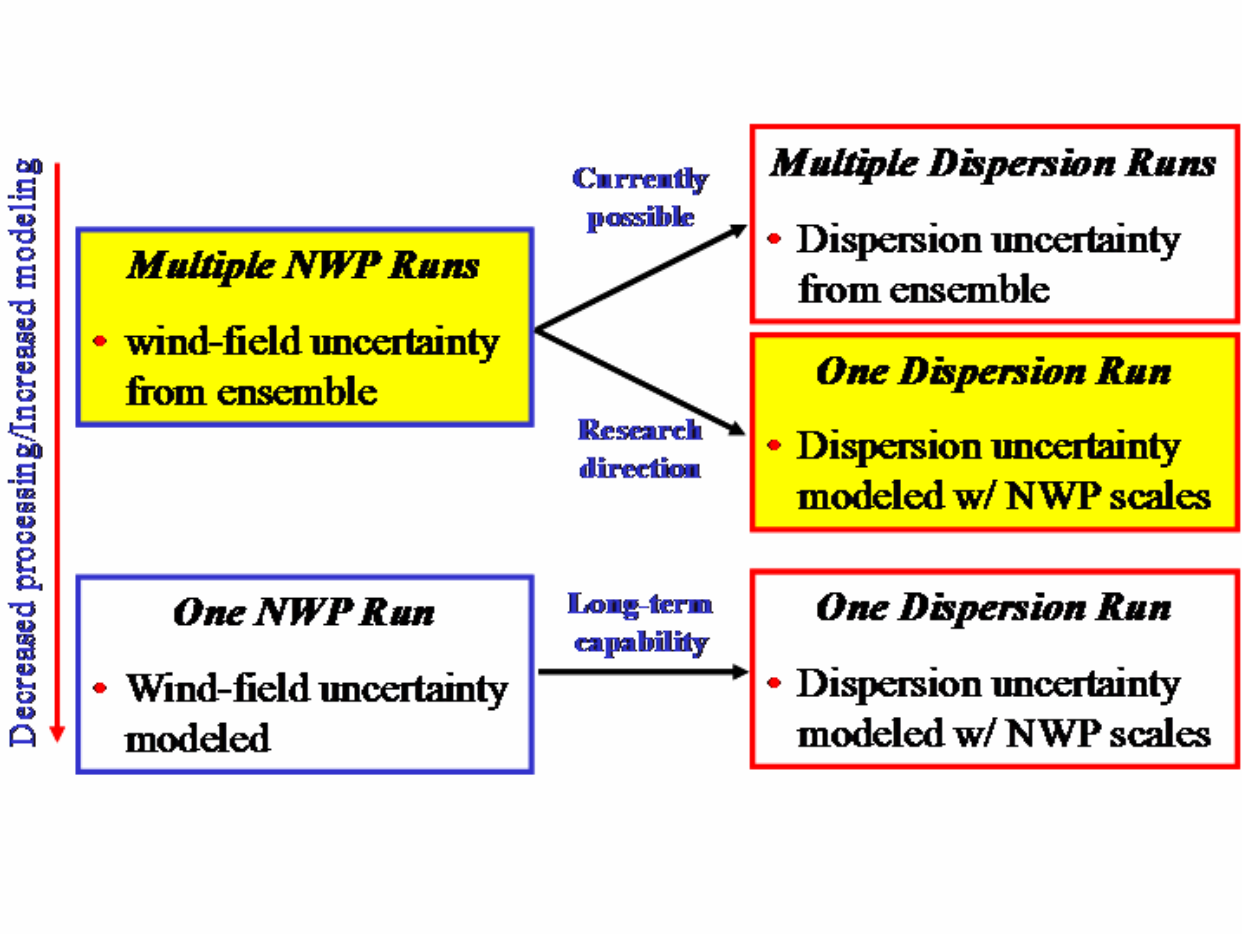


**Figure 2:** Accounting for large scale uncertainty in dispersion.

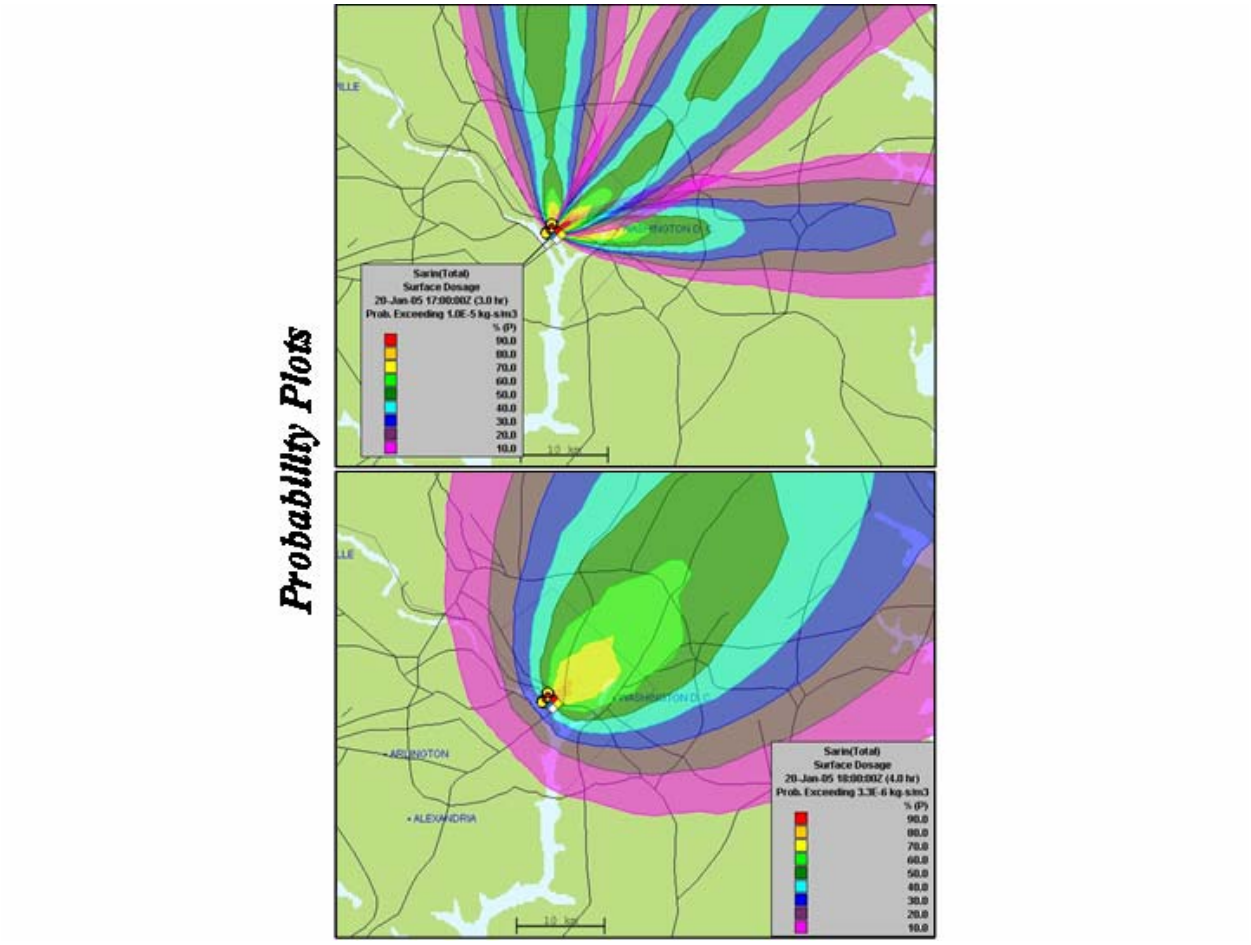


**Figure 3:** Large-scale uncertainty effects on dispersion: synthetic data showing dispersion plumes for 3 ensemble members of a wind field with high wind-direction uncertainty (upper panel) and a corresponding prediction with a representative wind field and parameterized uncertainty scales (lower panel).

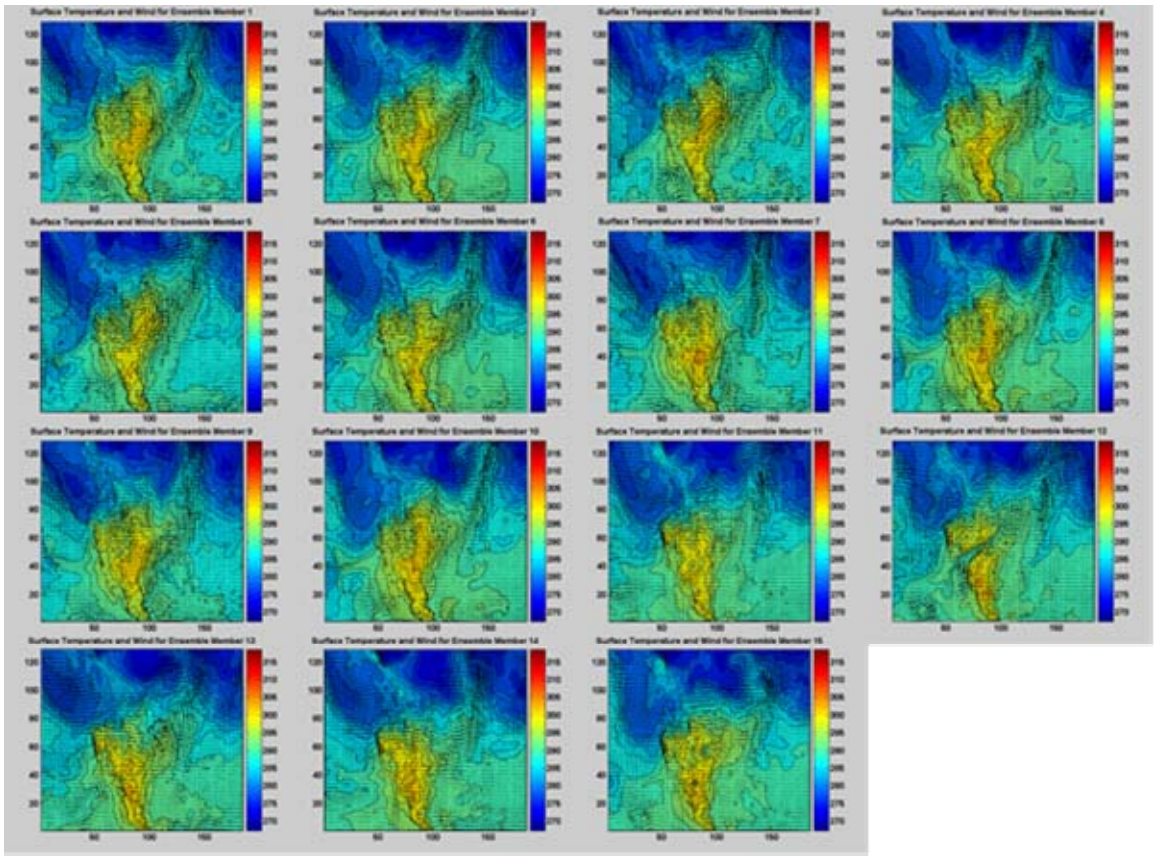

**Figure 4:** Wind vectors and surface temperature contours for 15 members of the short-range-ensemble forecast for the United States.

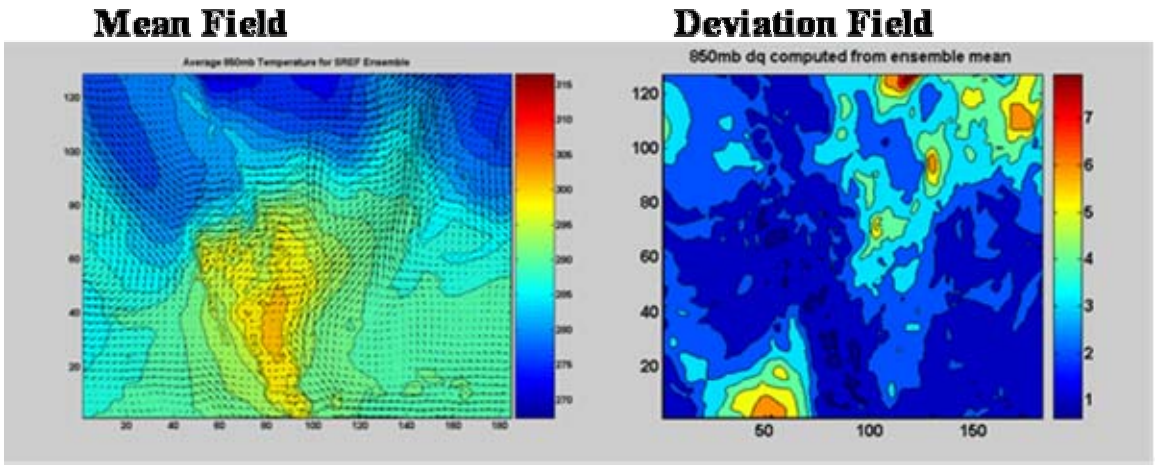


**Figure 5:** Mean field and characteristic velocity (m/s) data computed from the 15 member SREF ensemble.

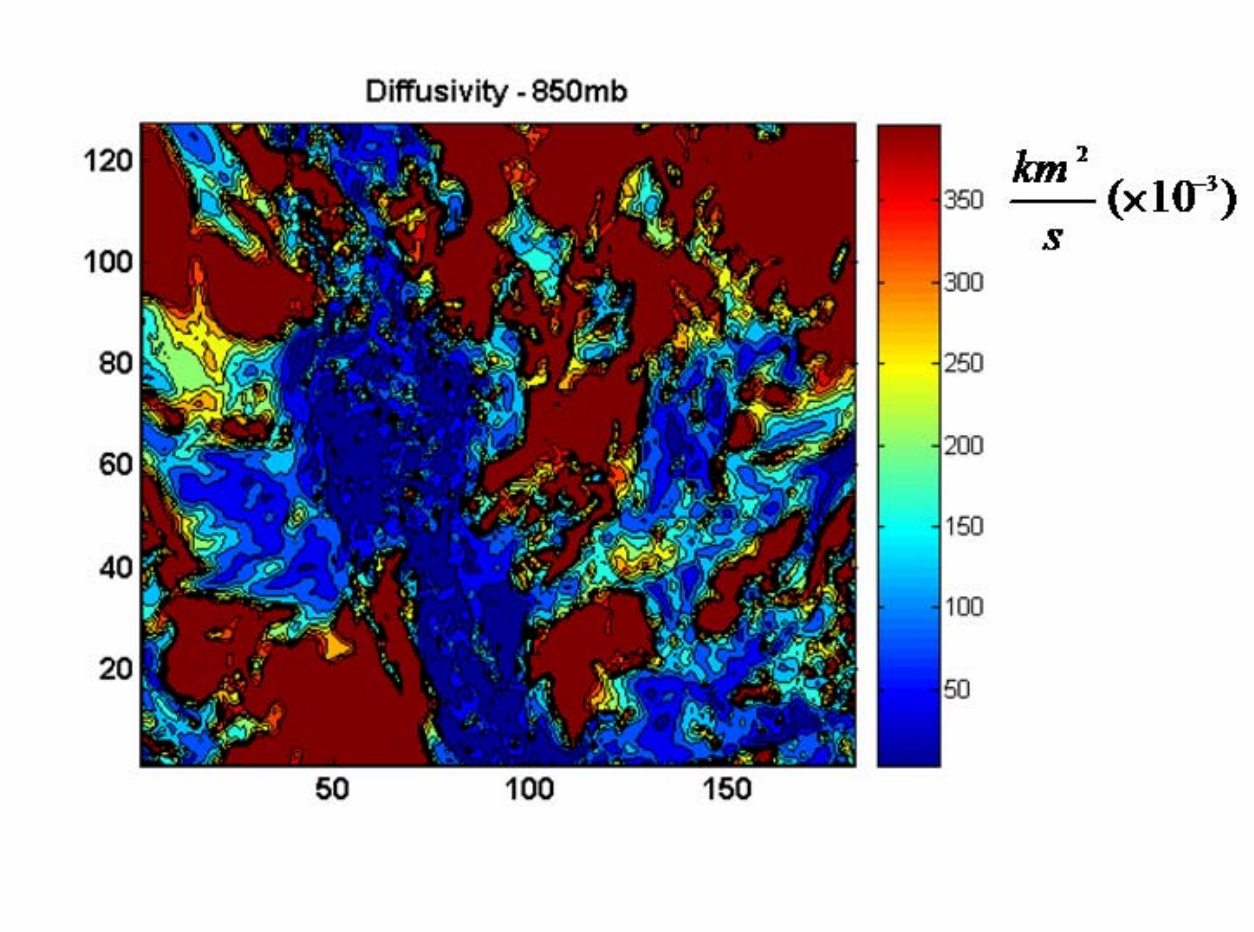


**Figure 6:** Large-scale diffusivity, $\nu_L$, computed from the SREF data.

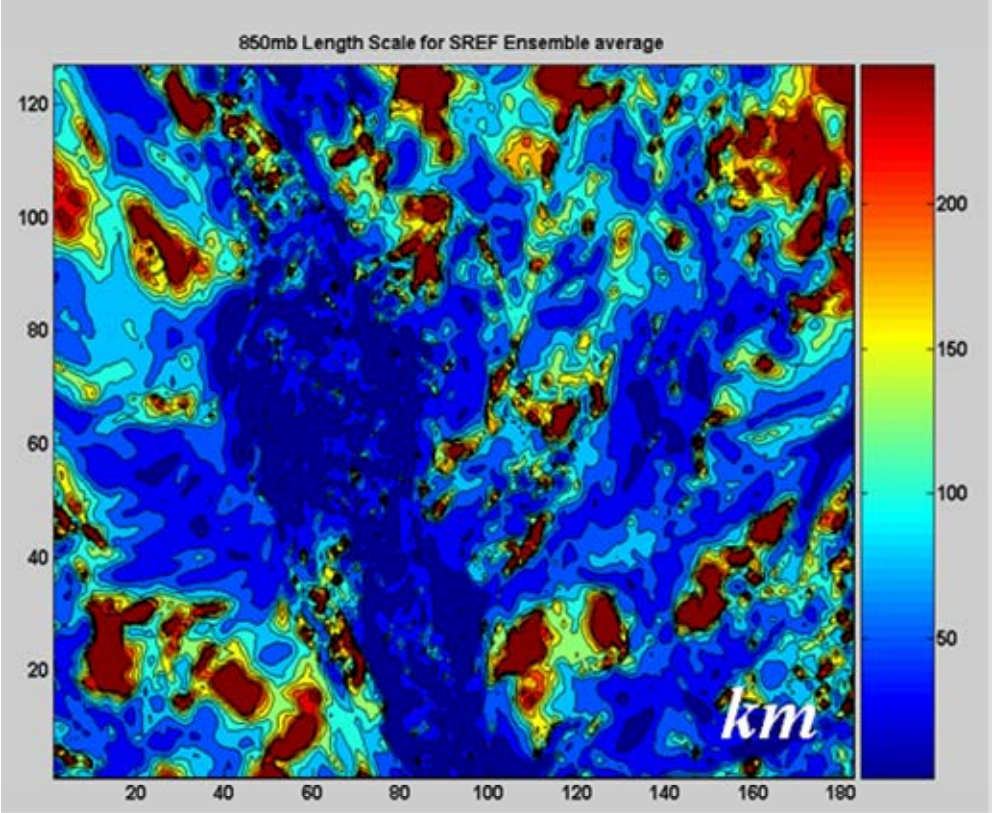


**Figure 7:** Large scale uncertainty mixing length, $\ell_L$ (km).